CZECH TECHNICAL UNIVERSITY IN PRAGUE
FACULTY OF ELECTRICAL ENGINEERING
DEPARTMENT OF PHYSICS

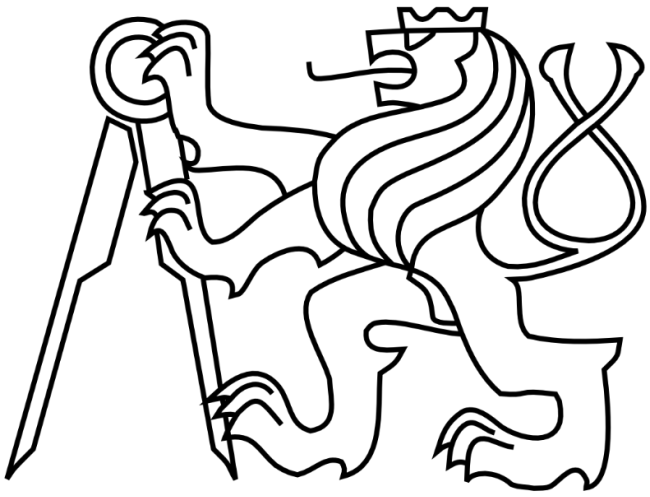

Bachelor Thesis

Elektronická detekce léčiva pomocí interdigitálnich senzorů pokrytých nanočásticemi

Electronic detection of drugs by nanoparticles covered interdigitated sensors

Author: Rustambek Bekmukhamedov
Supervisor: RNDr. Ilona Ali Bláhová, Ph.D

Prague 2018

BACHELOR'S THESIS ASSIGNMENT

I. Personal and study details

Student's name: **Bekmukhamedov Rustambek** Personal ID number: **427554**

Faculty / Institute: **Faculty of Electrical Engineering**

Department / Institute:

Study program: **Electrical Engineering and Computer Science**

II. Bachelor's thesis details

Bachelor's thesis title in English:

Electronic Measurement by Nanoparticle Covered Interdigiteted Sensors

Bachelor's thesis title in Czech:

Elektronická měření pomocí interdigitálních senzorů pokrytých nanočásticemi

Guidelines:

1. Review topics connected to interdigitated sensors, nanoparticles, impedance measurement.
2. Familiarization with LCR meter, impedance measurement, impedance spectroscopy.
3. Measurements with different kinds of sensors, their comparison and evaluation models.

Bibliography / sources:

1. Arnault J. Ch.: Nanodiamonds, Elsevier, Eastbourne, UK, 2017, ISBN 978-0-323-43029-6
2. Macdonald D.: Reflections on the history of electrochemical impedance measurement, Elsevir, Electrochemica Acta 51 (2006), 1376-1388.

Name and workplace of bachelor's thesis supervisor:

RNDr. Ilona Ali Bláhová, Ph.D., Department of Physics, FEE

Name and workplace of second bachelor's thesis supervisor or consultant:

Date of bachelor's thesis assignment: **26.02.2018** Deadline for bachelor thesis submission: **12.06.2018**

Assignment valid until: **30.09.2019**

RNDr. Ilona Ali Bláhová, Ph.D. Supervisor's signature	Head of department's signature	prof. Ing. Pavel Ripka, CSc. Dean's signature

III. Assignment receipt

The student acknowledges that the bachelor's thesis is an individual work. The student must produce his thesis without the assistance of others, with the exception of provided consultations. Within the bachelor's thesis, the author must state the names of consultants and include a list of references.

Date of assignment receipt	Student's signature

© ČVUT v Praze, Design: ČVUT v Praze, VIC

Declaration

I hereby declare that this thesis is the result of my own work and that I have clearly stated all information sources used in the thesis according to “Methodological Instructions of Ethical Principle in the Preparation of University Thesis”.

In Prague, 04.06.2018 Signature .....…….

Acknowledgments

I would like to express my gratitude and appreciation for my supervisor RNDr. Ilona Ali Bláhová for her support and guidance throughout my Bachelor thesis. I would also like to thank my family for their continuous support during my studies and my friend Alex for his patience.

Abstract

This thesis is dedicated to the research and measurement of interdigitated sensors covered by nanoparticles, using electrochemical impedance spectroscopy. Theoretical background on nanoparticles, their productions and properties, as well as, information about the methodology of the impedance measurement principle is presented. The application of detonation diamonds and gold nanoparticles are discussed. The thesis contains results of the measurement of individual sensors with different coatings, their comparison and interpretation of the results through a model.

Keywords

Electric Impedance Spectroscopy; Nanodiamonds; Interdigitated sensors; Impedence sensors; Analyte detection; Gold nanoparticles.

Abstrakt

Obsahem této práce je využití elektrochemické impedanční spektroskopie pro měření interdigitálních senzorů, které jsou pokryty vrstvami nanočástic. V teoretické části je shrnuta výroba a vlastnosti nanočástic, dále je uveden popis měřící metody založené na principu impedanční spektroskopie. Je diskutováno využití detonačních nanodiamantů a zlatých nanočástic. Základem samotné práce je pak měření jednotlivých typů senzorů, které jsou pokryty různými vrstvami nanočástic, porovnání získaných výsledků a jejich interpretace za pomoci modelu.

Klíčová slova

Elektrochemická impedanční spektroskopie; Nanodiamanty; Interdigitální senzor; Impedanční senzor; Zlaté nanočástice.

List of Abbreviations

NP: Nanoparticle
DND: Detonation Nanodiamond
AC: Alternating current
DC: Direct current
PC: Personal Computer
MTAB: 16-merkaptohexadecyltrimethylamonium-bromid
AD: Alzheimer's Disease
CVD: Chemical vapor deposition
DUT: Device under test
AuNP: Gold nanoparticles
DMSO: Dimethylsulfoxide
EC: Equivalent circuit

Table of Contents

1. Introduction

Sensors are essential tools widely used for scientific, engineering and healthcare purposes. They extend our ability to gather valuable information about the changes occurring in our surrounding environment.

In healthcare, the ability to accurately measure physiological and chemical processes is fundamental to the development of new diagnostic and therapeutic methods. In order to carry out such measurements, specific tools are necessary to detect physiological and chemical changes and to transform these changes into a form that can easily be analyzed and processed. A biosensor is one such tool and can be defined as an analytical device which converts a biological response into an electrical signal.

Interdigitated biosensors play an important role in the measurement of chemical and physical properties in biological and clinical research. Label-free biosensors allows us to probe target molecule through changes in the electrical properties of the surface (e.g., dielectric constant, impedance) [4]. They are able to provide easy and fast drug content and concentration levels. In particular, impedance biosensors with different surface coating will be explored. The properties of these sensors can be altered and enhanced by coating the surface with nano-sized particles such as DNDs, AuNP.

Extensive research and development is being carried out on the application of DNDs and AuNP for drug sensing and drug delivery [3][5].

2. Sensors

The detection techniques used in biosensors can be broadly classified into label-based and label-free. Label-based detection relies on the specific properties of labels for detecting a particular analyte. In contrast, label-free detection is suitable for the target molecules that are not labeled or the screening of analytes which are not easy to tag. [1] Specificity or selectivity of a sensor for a given molecule is provided through chemical modification of the device's surface. The selectivity of the sensor for a given molecule is dependent on the quality of the surface functionalization method used.

In our case we use impedance based sensors. They are fabricated at TESLA Blatná a.s. The sensors in Fig.1 are made of ceramic substrate and gold electrodes. The electrodes are interdigitated and the gap between them is 25 μm. The overall size is 5.5 x 8.8 x 0.6 mm^2 [2]. Tab.1 lists the characteristics of the sensor.

Sensor platform BI2	
IDES: Line/Gap	25 µm / 25 µm
Structure of the multilayer	NiCr / Ni / Au
Connection	Ag wire Ø 0.25 mm
Lead Length	10 ± 2 mm
Temperature range	-30 ℃ to +200 ℃
Dimensions	5.5 x 8.8 x 0.6 mm

Tab 1. IDT sensor specifications.

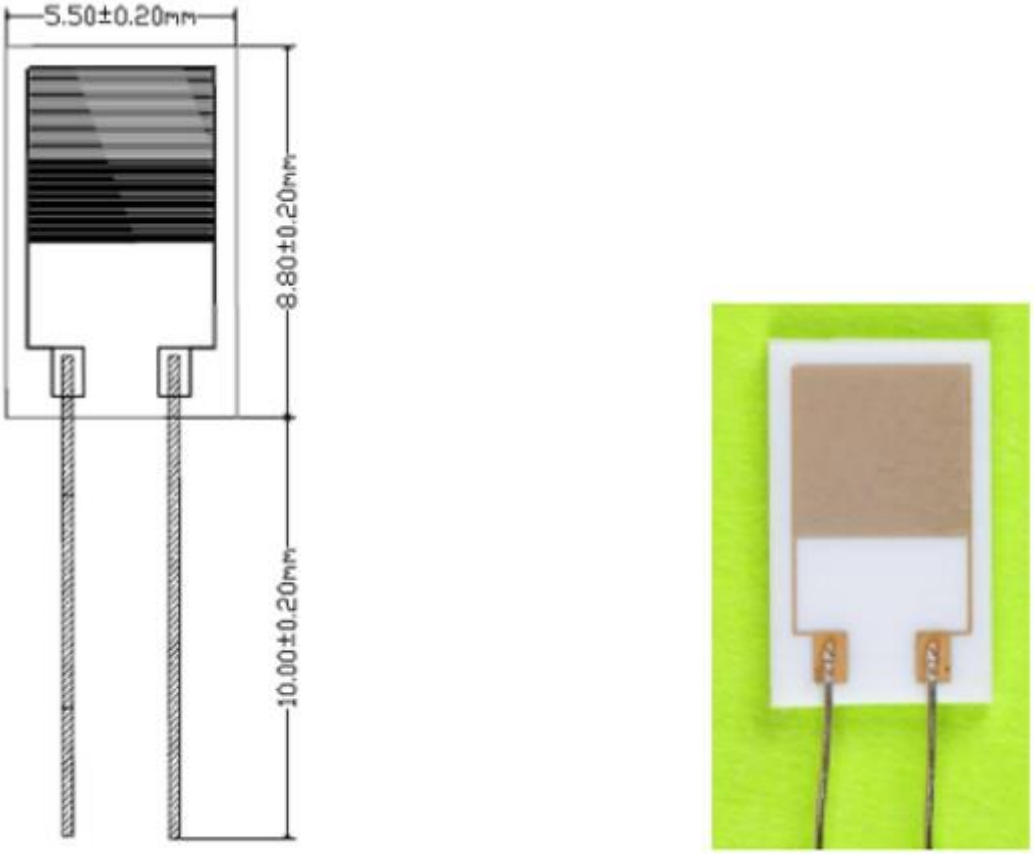

Fig 1. a) Dimensions of IDT sensor, b) Center-view of the IDT surface [1].

3. Nanoparticles

3.1 Nanodiamonds

Nanoscale diamond particles were first produced by detonation in the USSR in the 1960s, but they remained essentially unknown to the rest of the world until the end of the 1980s. Then, beginning in the late 1990s, a number of important breakthroughs led to wider interest in these particles, which are now known as nanodiamonds. First, colloidal suspensions of individual diamond particles with diameters of 4–5 nm ('single-digit' nanodiamonds) became available. Second, researchers started to use fluorescent nanodiamonds as a non-toxic alternative to semiconductor quantum dots for biomedical imaging [2]. Third, nanoscale magnetic sensors based on nanodiamonds were developed [2]. Fourth, the chemical reactivity of the surface of nanodiamonds allowed a variety of wet and gas chemistry techniques to be employed to tailor the properties of nanodiamonds for use in composites and also for other applications, such as attaching drugs and biomolecules [2]. Fifth, new environmentally friendly purification techniques were developed, and these allowed high purity nanodiamond powders with controlled surface chemistry to be produced in large volumes at a low cost [2]. Finally, nanodiamond was found to be less toxic than other carbon nanoparticles and, as a result, is currently being considered for applications in biomedical imaging, drug delivery and other areas of medicine [2].

Nanodiamonds combine many properties of bulk diamond like chemical inertness, wide-band gap electronic properties, excellent thermal conductivity, and outstanding mechanical behavior for their high specific surface area, which could reach 400 m^2/g for nanodiamonds produced by detonation synthesis [2].

The properties observed at nanoscale are significantly influenced by factors like the size and the shape of nanodiamonds, the nature and the concentration of impurities, the presence of structural defects, and the surface chemistry of outershells.

Several parameters of diamond are unique like high electron and hole mobilities, both of them approximately 2000 $\mathrm{cm}^2 \cdot \mathrm{Vs}^{-1}$, thermal conductivity of 25 $\mathrm{W} \cdot \mathrm{cm}^{-1} \cdot \mathrm{K}^{-1}$, electric breakdown field of 10^7 $\mathrm{V} \cdot \mathrm{cm}^{-1}$, hardness of 10^4 $\mathrm{kg} \cdot \mathrm{mm}^{-2}$, and Debye temperature of 1860 K [3]. At present time, diamond is available in single-, poly-, nano-, and ultra-nano-crystalline structure. There are several techniques, to fabricate diamond artificially. The High Pressure High Temperature (HPHT) technique, plasma-discharge-

stimulated chemical vapor deposition methods, and the hot-filament technique have been developed during the last 60 years. The most promising are optical applications (e.g infrared windows, lenses, ATR units, X-ray windows), thermal applications (heatspreaders, laser submounts, X-ray targets), mechanical applications (cutting tools, scalpels, knives, length gauge tips, wear resistant componenet, e.g for textile machines, inserts for dresser tools), electro-chemical applications (electrodes, electro-chemical detectors, bio-chemical sensors), radiations sensors (ionizing radiation detectors/dosimeters, fluorescence beam monitors), biolabels, and drug delivery componenets (diamond nanoparticles) [3]. General properties of a diamond are listed in Tab 2.

Properties/Materials	Diamond	Si	4H-SiC	GaN
Bandgap (eV)	5.47	1.12	3.26	3.5
Electron Mobility (cm^2/Vs) bei 300K	1,900-2,300	1,500	900	1,250
Hole Mobility (cm^2/Vs) bei 300K	1,500-2,300	600	100	200
Dielectric Constant	5.7	11.9	9.7	9.5
Thermal Conductivity	25	1.48	4.9	1.3
Electron Saturation Velocity (10^7 cm/s)	2.7	1	2.7	2.7
Breakdown Field	100	3	30	30
Debye Temperature (K)	1,860	645	1,200	608
Hardness (kg/mm^2)	10,000	1,000	4,000	

Tab 2. General properties of a diamond compared to other semiconducting materials [2]

3.1.1 Production of Nanodiamonds

To this day, numerous production methods have been invented, including the detonation technique, laser ablation, high-energy ball milling of diamond microcrystals grown at high static pressure and high-temperature (HPHT), chemical vapor deposition (CVD), microplasma-assisted nanodiamond formation from ethanol vapor at atmospheric pressure, chlorination of carbides, ion irradiation of graphite, electron irradiation of carbon onions, and ultrasound cavitation [2].

The most widely used of these types of nanodiamonds are those of detonation synthesis (DNDs), produced by detonation of carbon -containing explosives, and HPHT nanodiamond particles, obtained by milling of micron-size HPHT particles shown in Fig.2 [2].

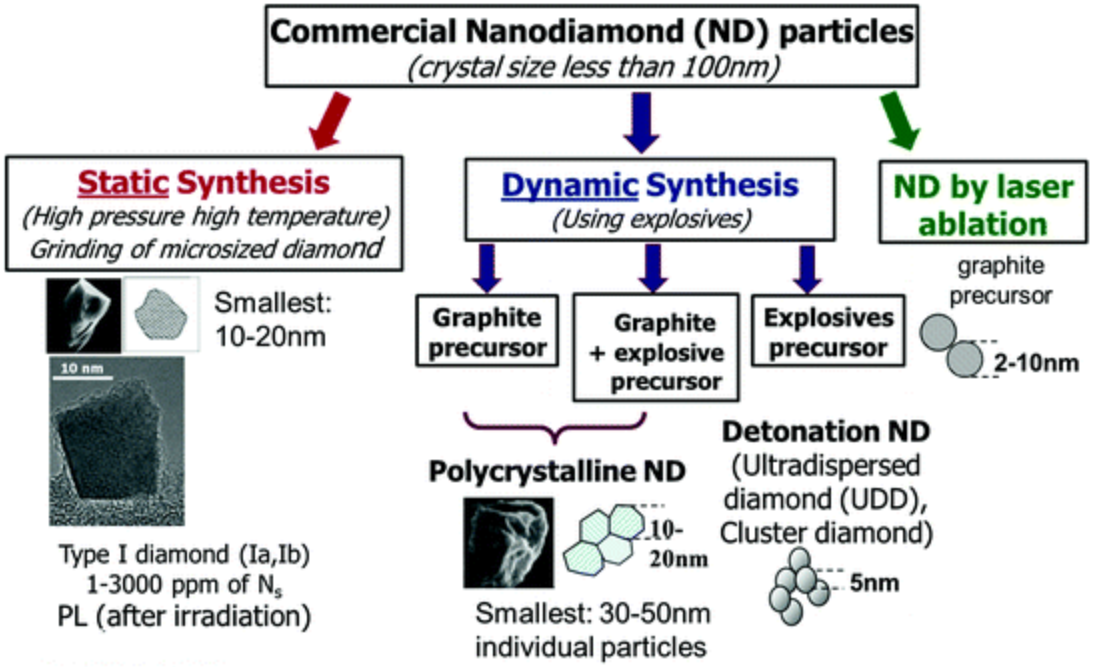

Fig 2. Summary of types of commercial nanodiamond [2].

To synthesize nanodiamonds, explosives with a negative oxygen balance (for example a mix of 60 wt% TNT ($C_6H_2(NO_2)_3CH_3$) and 40 wt% hexogen ($C_3H_6N_6O_6$)) are detonated in a closed metallic chamber in an atmosphere of N_2, CO_2 and liquid or solid H_2O. After detonation, diamond-containing soot is collected from the bottom and the walls of the chamber (Fig. 1a). [3]

Fig. 3b depicts phase diagram showing that the most stable phase of carbon is graphite at low pressures, and diamond at high pressures, with both phases melting when at temperatures above 4,500 K (with the precise melting temperature for each phase depending on the pressure). The phase diagrams for nanoscale carbon are similar, but the liquid phase is found at lower temperatures. During detonation, the pressure and temperature rise instantaneously, reaching the Jouguet point (point A), which falls within the region of liquid carbon clusters of 1–2 nm in size for many explosives. As the temperature and pressure decrease along the isentrope (red line), carbon atoms condense into nanoclusters, which further coalesce into larger liquid droplets and crystallize. When the pressure drops below the diamond–graphite equilibrium line, the growth of diamond is replaced by the formation of graphite. [3]

Fig. 3c shows the schematic of the detonation wave propagation showing (I) the front of the shock wave caused by the explosion; (II) the zone of chemical reaction in which the explosive molecules decompose; (III) the Chapman–Jouguet plane (where P and T correspond to point A in Fig. 2b, indicating the conditions

when reaction and energy release are essentially complete); (IV) the expanding detonation products; (V) the formation of carbon nanoclusters; (VI) the coagulation into liquid nanodroplets; and (VII) the crystallization, growth and agglomeration of nanodiamonds. [2]

The decomposition reaction of explosive molecules and formation of free carbon (for an explosive with negative oxygen balance) is described according to the formula (1) [3].

$$CNOH \rightarrow N_2 + H_2O + CO + CO_2 + C \quad (1)$$

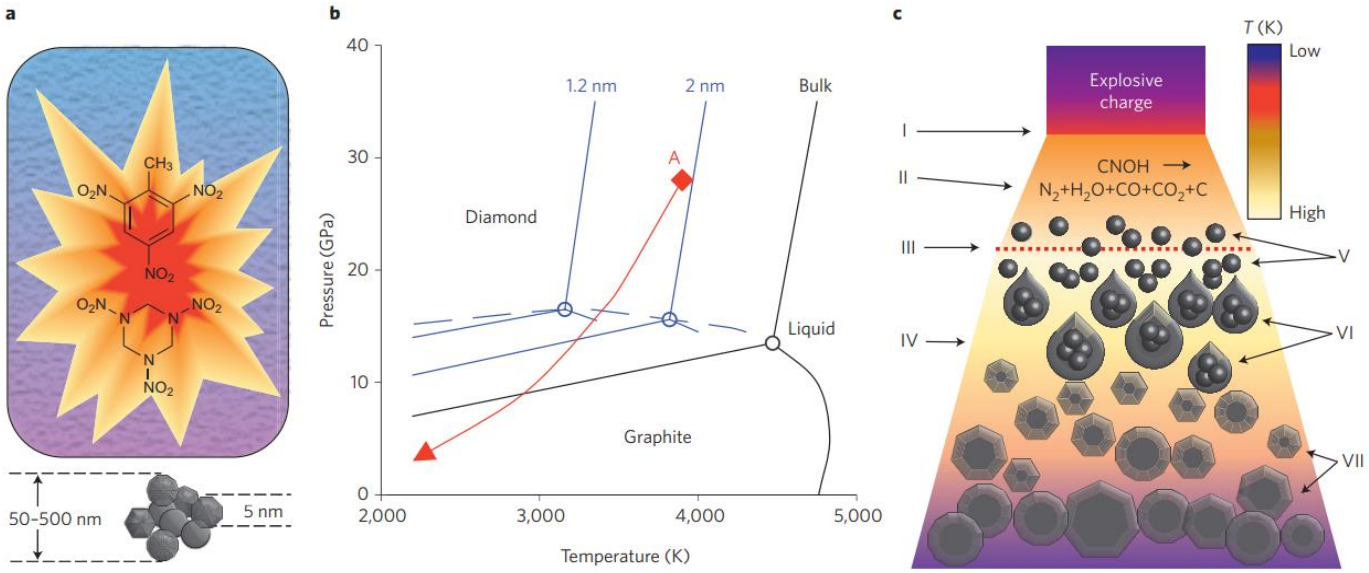

Fig 3. Detonation synthesis of nanodiamonds [3].

Under suitable conditions, shock waves produced by explosives in confined volumes for sufficient durations can create high pressure (~20-200 GPa) and high temperature (> 2000 K) that will result in partial conversion of graphite into nanometer-sized diamond grains (~20 nm);

Annealing under different atmospheres may be used to modify the surface properties of DND. The ND particles used on the sensors surface are hydrogen terminated and oxygen terminated (H-DND and O-DND respectively).

3.2 Gold nanoparticles

Gold nanoparticles (AuNP) have been widely used in bio nanotechnology based on their unique properties and multiple surface functionalities. The ease of AuNP functionalization provides a versatile platform for nanobiological assemblies with oligonucleotides, antibodies, and proteins [9].

In diagnostics, the binding event between the analytes and the AuNP can alter the physicochemical properties of AuNP such as surface plasmon resonance, conductivity, and redox behavior, leading to detectable signals [9].

AuNP are generally synthesized by chemical reduction of Au salts in aqueous-phase, organic-phase, or mixed-phase solutions. The most difficult aspect of this synthesis is to control the reactivity of the AuNP surface during particle growth, since the surface energy is quite high. Controlled synthesis of AuNP requires the use of stabilizing agents, such as citrate or thiolated species, that bind to the particle surface to control growth and to prevent aggregation. Numerous methods have been reported for creation of biomolecule-Au-nanoparticle conjugates either during or after Au-nanoparticle synthesis. Commercial reagents are now available for conjugation of biomolecules to Au nanoparticles. One of the primary reasons for the intensive research into biomolecule-Au-nanoparticle conjugates is that biomolecules in this environment are generally stable and retain their biological activity. [5]

4. Electrochemical Impedance Spectroscopy

The measurements done on the interdigitated sensors is based on the electrochemical impedance spectroscopy for analyte detection. The EIS has proved itself as a powerful tool for studying the mechanisms of electrochemical reactions. For measuring the impedance, the LCR device utilized in the laboratory, applies an AC voltage probe (approximately 1V), at different frequencies, and the current response is determined. The in-phase current response determines the real (resistive) part of the impedance, while the out-of-phase current response determines the imaginary (capacitive) component. The AC probe voltage should be small enough so that the system response is linear, allowing simple equivalent circuit analysis.

EIS is quite powerful, in that it is capable of characterizing physicochemical processes of widely differing time constants, sampling electron transfer at high frequency and mass transfer at low frequency. [8]

Impedance results are commonly fitted to equivalent circuits of resistors and capacitors, such as Randels circuit shown if Fig. 4., which is often used to interpret simple electrochemical processes. From this EC we can obtain the Nyquist plot shown in Fig. 5which allows us to see into the system dynamics.

In Figs. 4 and 5, R_{ct} is the charge-transfer resistance, which is inversely proportional to the rate of electron transfer; C_d is the double-layer capacitance; R_S is the solution-phase resistance; and, Z_W is the Warburg

impedance, which arises from mass-transfer limitations. If an analyte affects one or more of these equivalent circuit parameters and these parameters are not affected by interfering species, then impedance methods can be used for analyte detection. R_S arises primarily from the electrolyte resistance and is analytically useful mainly in conductivity sensors. [5]

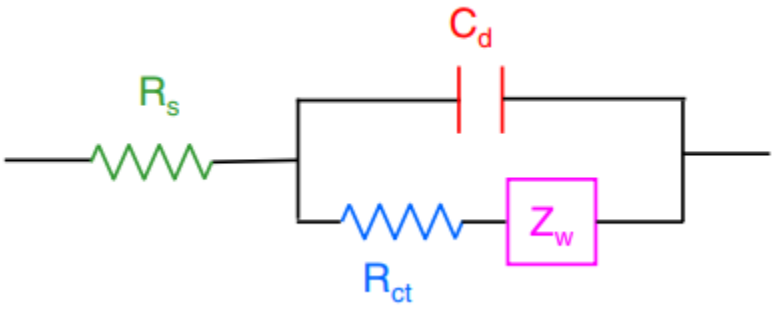

Fig 4. Randels Equivalent circuit for a simple electrochemical system [5].

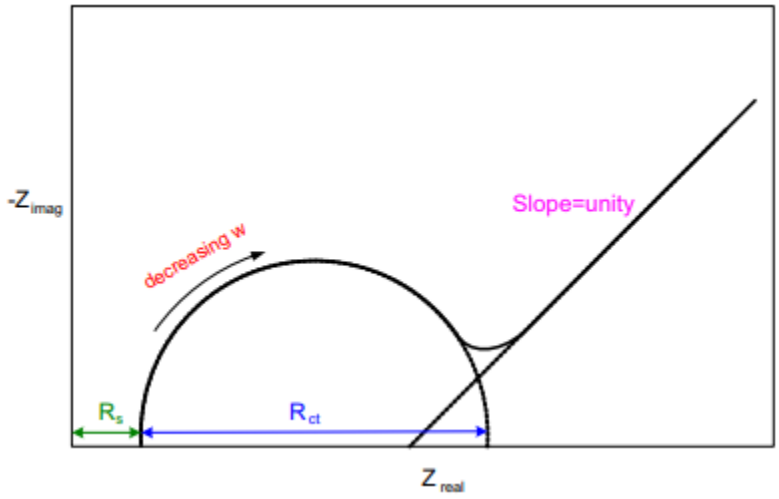

Fig 5. Nyquist plot produced by Randels Equivalent Circuit [5].

The equivalent circuit elements in Figs. 4 that are most often useful for analyte detection are R_{ct} and C_d [5]. The measured capacitance usually arises from the series combination of several elements, such as analyte binding (C_{an}) to a sensing layer (C_{sens}) on an Au electrode (C_{Au}) [5]. In this case, the measured capacitance is:

$$\frac{1}{C_d} = \frac{1}{C_{Au}} + \frac{1}{C_{sens}} + \frac{1}{C_{an}} \tag{2}$$

In many cases, the capacitance at the Au electrode-sensing layer interface is large and can be neglected. For analyte binding (R_{an}) to a sensing layer (R_{sens}) on an Au electrode (R_{Au}), the measured resistance is:

$$R_{ct} = R_{Au} + R_{sens} + R_{an} \tag{3}$$

The resistance at the interface between the Au electrode and the sensing layer is typically negligible. Impedance sensing is most useful for large species that significantly disturb the sensing interface. So R_{ct} can be used to monitor the concentration of analytes.

Warburg impedance, created by diffusion, depends on the frequency of the potential disturbance. At high frequencies, the Warburg impedance is small since diffusing reactants don't have to move very far. At low frequencies, the reactants have to diffuse farther, increasing the Warburg-impedance. [8]
The equation of the Warburg impedance for bounded diffusion layer has the form [8]:

$$Z(j\omega) = R_{ct}\left[1 + \frac{k_f \tanh\left(\delta_N\sqrt{j\omega D_O^{-1}}\right)}{\sqrt{j\omega D_O}} + \frac{k_b \tanh\left(\delta_N\sqrt{j\omega D_R^{-1}}\right)}{\sqrt{j\omega D_R}}\right] \tag{4}$$

In which,

R_{ct} – Charge transfer resistance
δ_N – the ideal Nernst diffusion layer thickness
k_f and k_b – rate constants for the reaction in the forward and backward direction
D_O and D_R – diffusion coefficients of the oxidant and reductant species

On a Nyquist Plot the Warburg impedance appears as a diagonal line with a slope as show in Fig. 5, for low frequencies. As illustrated in Fig. 5, the plot starts linear for lower frequencies and becomes non-linear or circular shaped for higher frequencies.

5. Impedance measurement device

Impedance measurement data were collected using the HIOKI IM 3536 LCR Meter (Fig. 6). The LCR Meter interfaces with a PC through USB for data acquisition and processing. The device ships with standard application software for saving measurement data as Microsoft Excel and text files (CSV format) using its USB interface. Since we are measuring frequency sensitive devices, the LCR meter is capable of sweeping through multiple frequency, voltage and current values. The specifications of the device are given in Tab.3.

Fig 6. HIOKI IM 3536 LCR Meter [12].

Measurement Modes	LCR, Continuous Testing
Measurement Parameters	Z, Y, θ, X, G, B, Q, Rdc, R, L, C, D (tanδ), σ, ε
Measurement range	100 mΩ to 100 MΩ
Basic accuracy	Z ±0.05% rdg. θ: ±0.03° (for range: 1 mΩ to 200 MΩ)
Measurement frequency	4 Hz to 8 MHz (5 digits setting resolution, minimum resolution 10 mHz)
DC bias measurement	DC voltage 0 V to 2.50 V (10 mV resolution)
Output impedance	Normal mode: 100 Ω, Low impedance high accuracy mode: 10 Ω

Measurement signal level	[Normal mode: V mode/CV mode] 4 Hz to 1.0000 MHz: 10 mV to 5 Vrms (maximum 50 mArms) 1.0001 MHz to 8 MHz: 10 mV to 1 Vrms (maximum 10mArms) [Low impedance high accuracy mode: V mode/CV mode] 4 Hz to 1.0000 MHz: 10 mV to 1 Vrms (maximum 100 mArms) [Normal mode: CC mode] 4 Hz to 1.0000 MHz: 10 μA to 50 mArms (maximum 5 Vrms) 1.0001 MHz to 8 MHz: 10 μA to 10 mArms (maximum 1 Vrms) [Low impedance high accuracy mode: CC mode] 4 Hz to 1.0000 MHz: 10 μA to 100 mArms (maximum 1 Vrms) [DC resistance measurement] Measurement signal level: Fixed at 1 V

Tab 3. HIOKI IM 3536 LCR Meter Specifications [11].

The impedance is measured by applying a constant AC voltage of about 1 V_{rms} with variable frequency between the terminals H_p and L_p, and reading current changes at the terminals H_c and L_c (Fig. 7). Since the voltage across the DUT - V_{DUT} , is dependent on frequency, mainly because of C_d (Fig. 4), it is defined as:

$$V_{DUT} = \frac{Z_{DUT}}{R_o + Z_{DUT}} \cdot V_0 \tag{5}$$

$$Z_{DUT} = \frac{X_c \cdot (R_{ct} + Z_w)}{X_c + R_{ct} + Z_w} \tag{6}$$

$$X_c = \frac{1}{j\omega C_d} \tag{7}$$

Where

Z_{DUT} – impedance of our sensors

R_0 – output resistance of the LCR meter

V_0 – source voltage

X_c – reactance of the capacitor

The voltage detecting circuits inside the LCR meter will automatically monitor and adjust the DUT voltage, accordingly, in order to maintain a constant value.

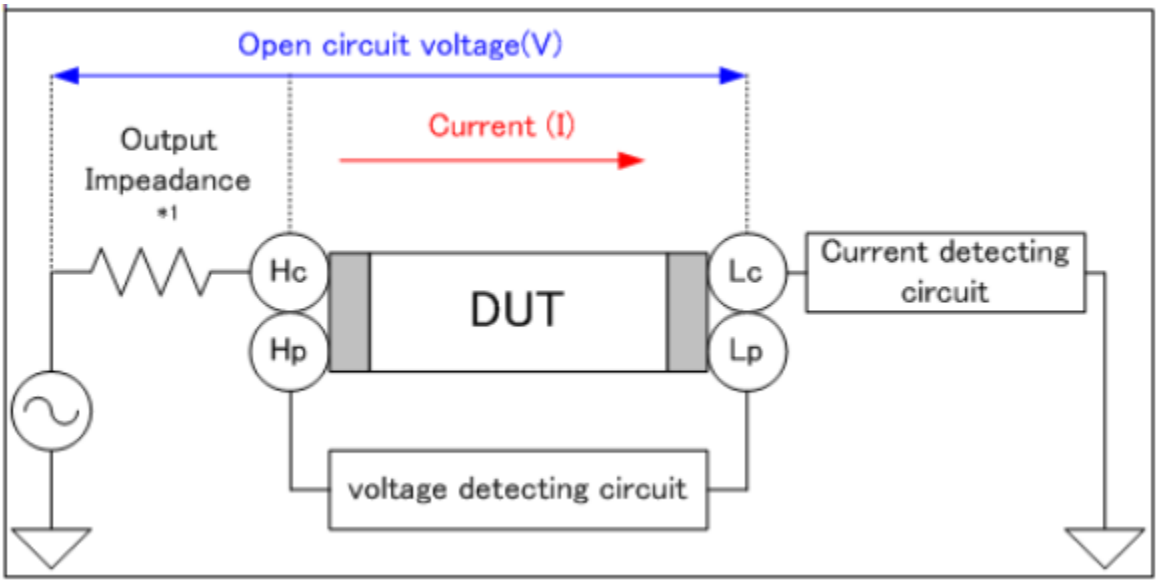

Fig 7. Simplified Diagram of measurement of the Device under Test [11].

5.1 Measurement Error Compensation

Because the sensors we are measuring cannot be connected directly the cables, it is necessary to eliminate the effects of the fixture's residual impedance and the cables. Conveniently, the LCR Meter is equipped with the following compensation functionality:

- Open and short compensation
- Load compensation
- Cable compensation

5.1.1 Open/Short Compensation

Open and short compensation functionality eliminates errors caused by the test fixture's and cables residual component. The DUT and measuring instrument that comprise a test fixture EC, as depicted in Fig. 8, where Z_S indicates the impedance in series with the DUT and Y_o indicates the admittance in parallel with the DUT.

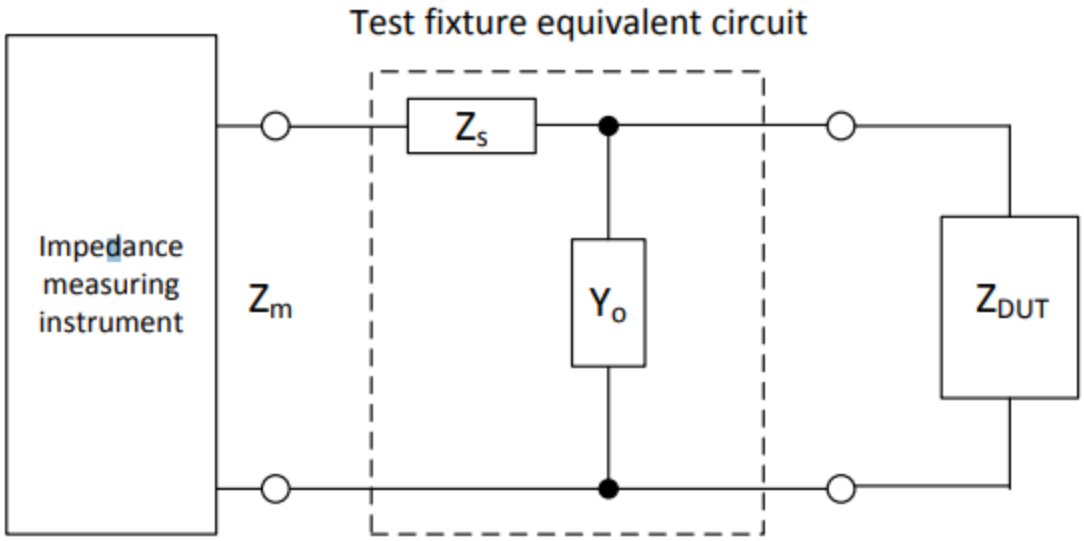

Fig 8. Test fixture equivalent circuit of the LCR Meter [12].

The DUT's impedance true value Z_{DUT} can be expressed as follows, where Z_m indicates the impedance that is measured at the measuring instrument's measurement terminals [12]:

$$Z_{DUT} = \frac{Z_m - Z_S}{1 - Y_0(Z_m - Z_s)} \tag{8}$$

By performing open and short compensation, it is possible to correct Z_m when Z_{DUT} is open (=Z_{om}) and Z_m when Z_{DUT} is shorted (= Zsm). Z_{om} and Z_{sm} can be calculated using the following formulas [12]:

$$Z_{om} = Z_S + \frac{1}{Y_0} \tag{10}$$

$$Z_{sm} = Z_S \tag{11}$$

Impedance measuring instruments calculate measured values using the following formula from the values obtained from Equations:

$$Z_{DUT} = \frac{(Z_{om} - Z_{sm})(Z_m - Z_{sm})}{Z_{om} - Z_m} \tag{12}$$

5.1.2 Load Compensation

Load Compensation. The load compensation procedure consists of measuring a component whose value is accurately understood and then calculating a compensation coefficient. Measured values can then be calculated by applying the compensation coefficient to observed values.

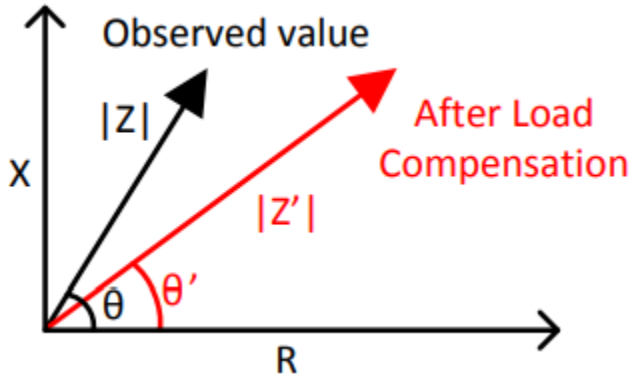

Fig 9. Load Compensation visualized in complex plane of impedance [12].

5.1.3 Cable Compensation

Cable Compensation. Cable length compensation comprises functionality for correcting errors that arise from coaxial cables' transmission characteristics. Extending the length of the cables between the measuring instrument and the DUT causes errors in the amplitude and phase of the signal applied to the DUT. This effect becomes more pronounced the higher the measurement frequency, and it can also introduce an error component into impedance measured values. [12]

Measurement terminal structure. When performing measurement with an impedance measuring instrument, it is necessary to establish contact with the DUT via probes or a fixture. Most impedance measuring instruments have four measurement terminals, and the method of connecting the instrument to the DUT varies with the probe and fixture structure as well as the shape of the measurement target. [12]

Two- terminal connection is the simplest connection type, as illustrated in Fig. 10. In our measurement the instrument's current signal path and voltage signal path are connected. Therefore, it is necessary to take into account some parasitic components as illustrated in Fig. 10 are listed in Tab. 4. [12]

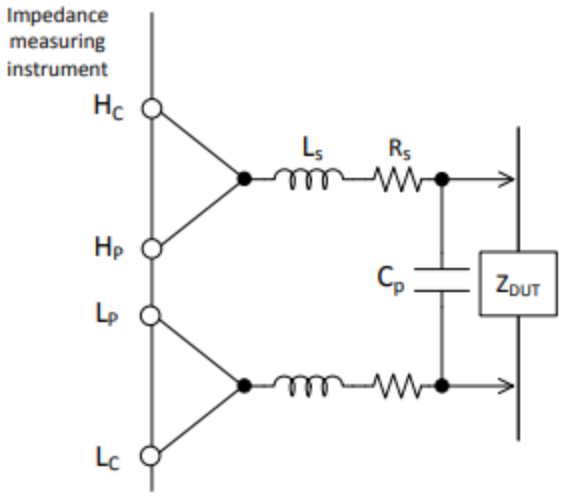

Fig 10. Diagram of two-terminal measurement of the LCR Meter [12].

Error Source		Effect
L_S	Parasitic inductance of cables and probes	Most affective when measuring low impedance at high frequency
R_S	Cables parasitic resistance	May affect if Z_{DUT} not greater than R_S
C_p	Parasitic capacitance between cables	Most affective when measuring high impedance at high frequency

Tab 4. Source of errors in two-terminal connections and their effects in the LCR Meter

6. Preparation of materials

6.1 Preparation of ND suspension

The DNDs were received from commercial producers in the form of dry powder as shown in Fig.11. Both H-DND (polyfunctional) and O-DND (oxidized and purified by annealing in the air at 450 ℃ for 30 min), were first mixed with of deionized water (10 mg of powder with 1ml H_2O). Next, the mixture is subjected to ultrasonication, with the ultrasonic horn set to 60-80% power, on and off time at 60% and 40%, for the duration of 1 hour. Afterwards, additional 1ml of H_2O was added, with the whole mixture consisting of 10 mg of DND and 2 ml of H_2O. Finally, the solution was processed in the centrifuge at 14500 RPM for the duration of 1 hour. Before application onto the sensor surface, the suspension is diluted 10 times (Fig. 12).

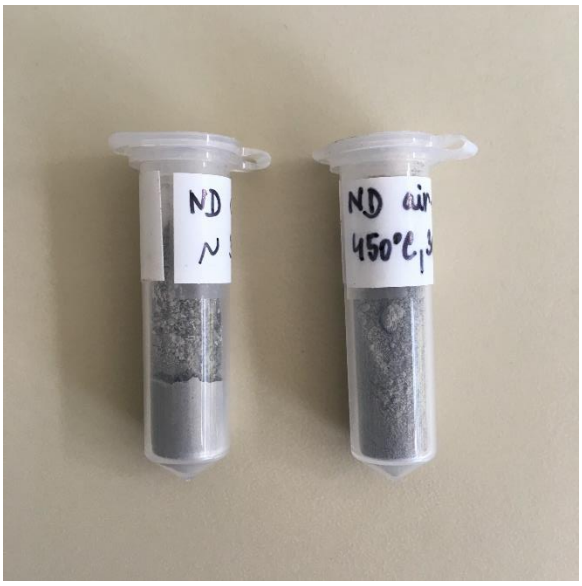

Fig 11. H-DND and O-DND samples in powder form.

Fig 12. Suspensions of O-DND and H-DND particles.

6.2 Colloidal solution of AuNP

Gold nanoparticles, purchased from British manufacturer “BBI Solutions”, are a suspension consisting of sub-micron gold nanoparticles suspended within a solvent (Fig. 13). According to the data sheet of the manufacturer [13] the Au particles have the mean diameter of 19.7 nm and the number of particles per ml is $7.00 \cdot 10^{11}$. Moreover, their website claims to provide improved consistency with <5% uneven shapes, which ensures even protein conjugation, which is proper for our needs.

Fig 13. Colloidal solution of AuNP.

6.3 MTAB

The purpose of MTAB is to functionalize the surface of the AuNP for inducing noncovalent bonding of the drug molecules. It was delivered from the Faculty of Nuclear Sciences and Physical Engineering in powder form. A 0.1 mmol solution is prepared, by mixing 0.8 mg of MTAB with 2 ml of H_2O, then diluted 10 times (Fig.14).

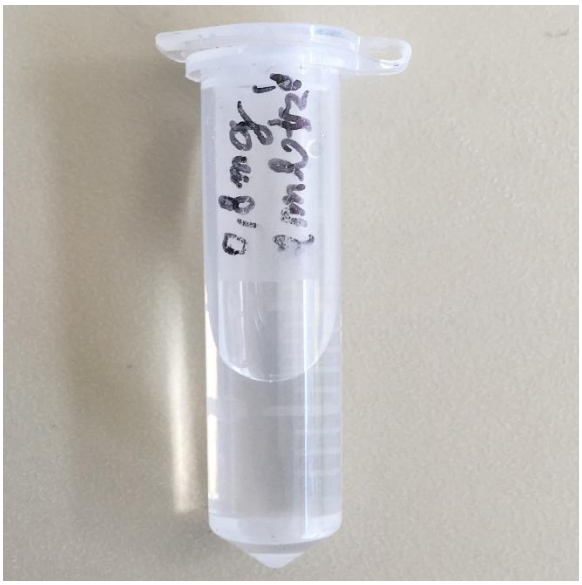

Fig 14. MTAB solution.

6.4 Anti-Alzheimer's disease drug

The analyte, which is being tested on the sensors, is an anti-AD agent, denoted as 1-EN-142. It was prepared at the University Hospital at Hradec Králove in cooperation with University of Defence. According to the research [14], it has been designed to target multiple components of the disease, as AD is characterized by multiple factors. The agent is mixed in DMSO solution (10% DMSO and 90% H_2O) (Fig. 15).

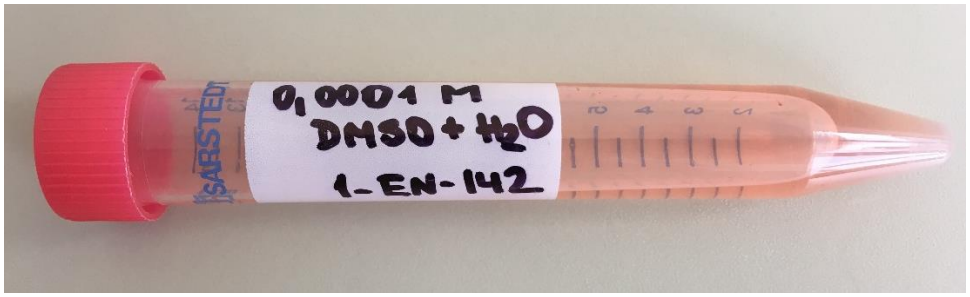

Fig 15. Anti-Alzheimer's disease drug solution.

7. Preparation of sensors for impedance measurement.

7.1 Application of individual layers onto the sensors

Before a layer is applied onto a new sensor, the sensor is rinsed with 1ml of 70% ethanol. Each layer is applied the following way:

a. **H-DND or O-DND**. 20 µl of the solution is dropped to the sensing surface and left on the hot plate set to 40 ℃ for 90 min.
b. **Au (separately or on top of the DNDs).** 20 µl dropped onto the sensor and left to dry on hot plate set to 40 ℃ for 90 min.
c. **MTAB**. 20 µl of the solution applied to the surface and left to dry at room temperature for 30 min. Afterwards, the surface is rinsed with 1 ml of H_2O. Following the rinse, the next layer is applied immediately, to avoid degradation.
d. **Anti – AD agent**. 20 µl of the solution applied to the sensor. Then left to dry on hot plate, set to 40 ℃, for 240 min.

After the drying of the final layer, the surface is rinsed by 20 µl of H_2O, followed by 1 ml of methanol, this sequence is repeated one more time, before finishing rinsing with 20 µl of H_2O. The sensors are left to dry on hot plate, set to 40 ℃, before proceeding to impedance measurement.

8. Measurement Results

Measurement of impedance for sensors with coatings listed in Tab. 5, were performed in chamber (Fig. 16 and 17) and in HP Test Fixture 16074C (Fig.18). The 4 terminals of the cables coming from the LCR meter are soldered together into two-terminals to the sensor holder inside the chamber (Fig. 17). The grounding is connected to the metal enclosure.

Sensor No.	Coating
1	Empty
2	Ref: MTAB / EN
3	H-DND / EN
4	H-DND / AuNP / EN
5	O-DND / EN
6	O-DND / AuNP / EN
7	AuNP / EN
8	H-DND
9	H-DND / AuNP
10	AuNP
11	O-DND
12	O-DND / AuNP
36	O-DND / AuNP / MTAB / EN

Tab 5. Sensors with different layers of coatings.

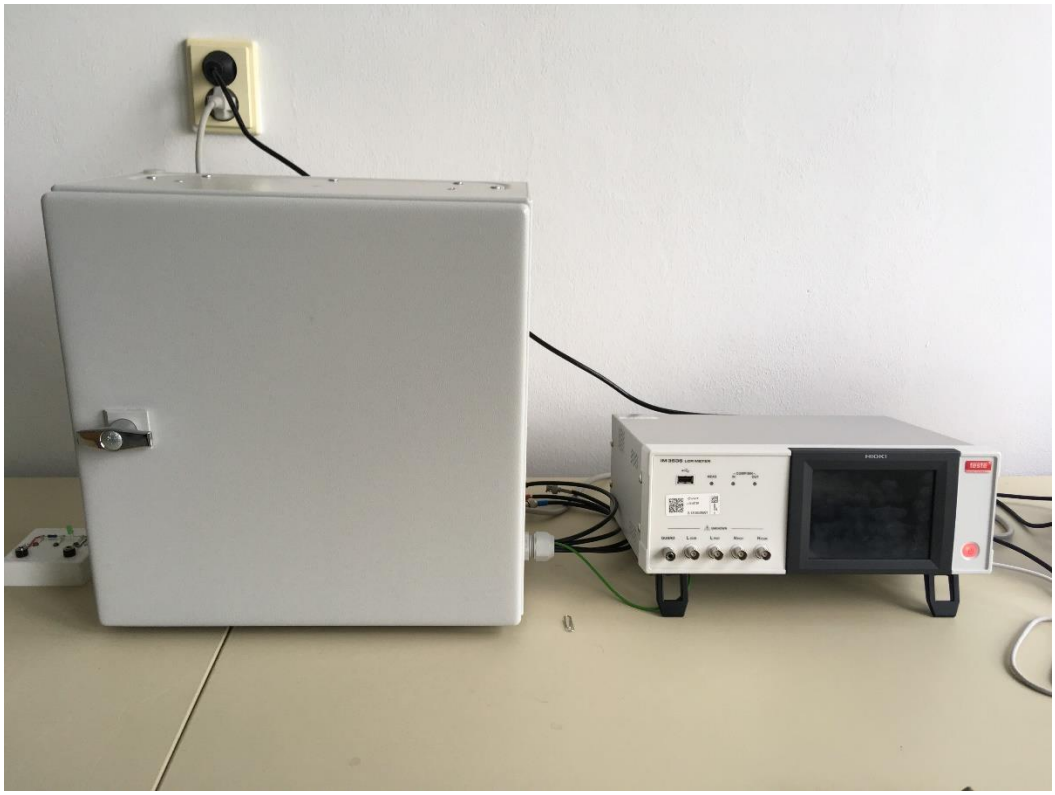

Fig 16. Chamber (left) for the measurement impedance with LCR Meter (right).

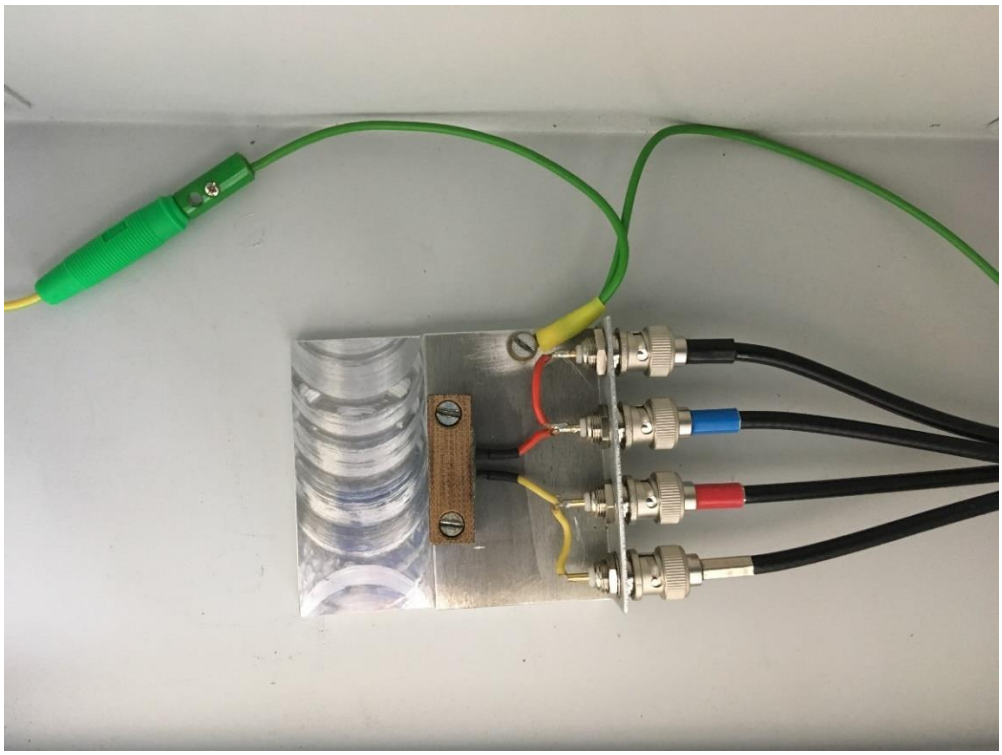

Fig 17. The measurement holder inside the chamber.

Fig 18. Test Fixture connect to the LCR Meter.

The parameters of the HIOKI IM3536 were setup as shown in Tab. 6. Before the measurement, the LCR meter was calibrated for open and short. In case of chamber measurement, the cable length for compensation was set to 1m, and in case of test fixture – 0 m. PC application was set to make a sweep measurement starting from 42 Hz till 5 MHz with 50 data points and scale set to logarithmic. The interval between sweeps was set to 0 s. Number of measurements was set to 3, with 1 s interval between them, in order to check repeatability. The measured data was output into an Excel sheet and processed. After confirming the repeatability, the data from the initial time was taken into consideration. Measurement was done as quickly as possible in order to avoid the effects of evaporation, while still preserving the accuracy of the measurement.

AC SETTINGS	
VOLTAGE	1V
LIMIT	OFF
RANGE	AUTO
LOW Z	OFF
SPEED	MEDIUM
AVG	OFF
DELAY	0 s
TRIG SYNC	OFF
DC BIAS	OFF

Tab 6. HIOKI IM3536 LCR Meter Setup Parameters for measurement.

Fig.18-21 shows the Nyquist plots obtained from the measurement of individual sensor types. Overall, the impedance measurements obtained in test fixture, displays a higher impedance, which is evidenced by a wider semicircle. This difference may be the result of the absence of load compensation which requires the true value of the DUT, as well as, the effect of the soldered joints between the cables and the sensor holder. This requires furthermore investigation. However, the measurement made in chamber in Fig. 6, provided consistent and improved separation between individual sensor types. Therefore, comparison and conclusions were made over the data from the chamber.

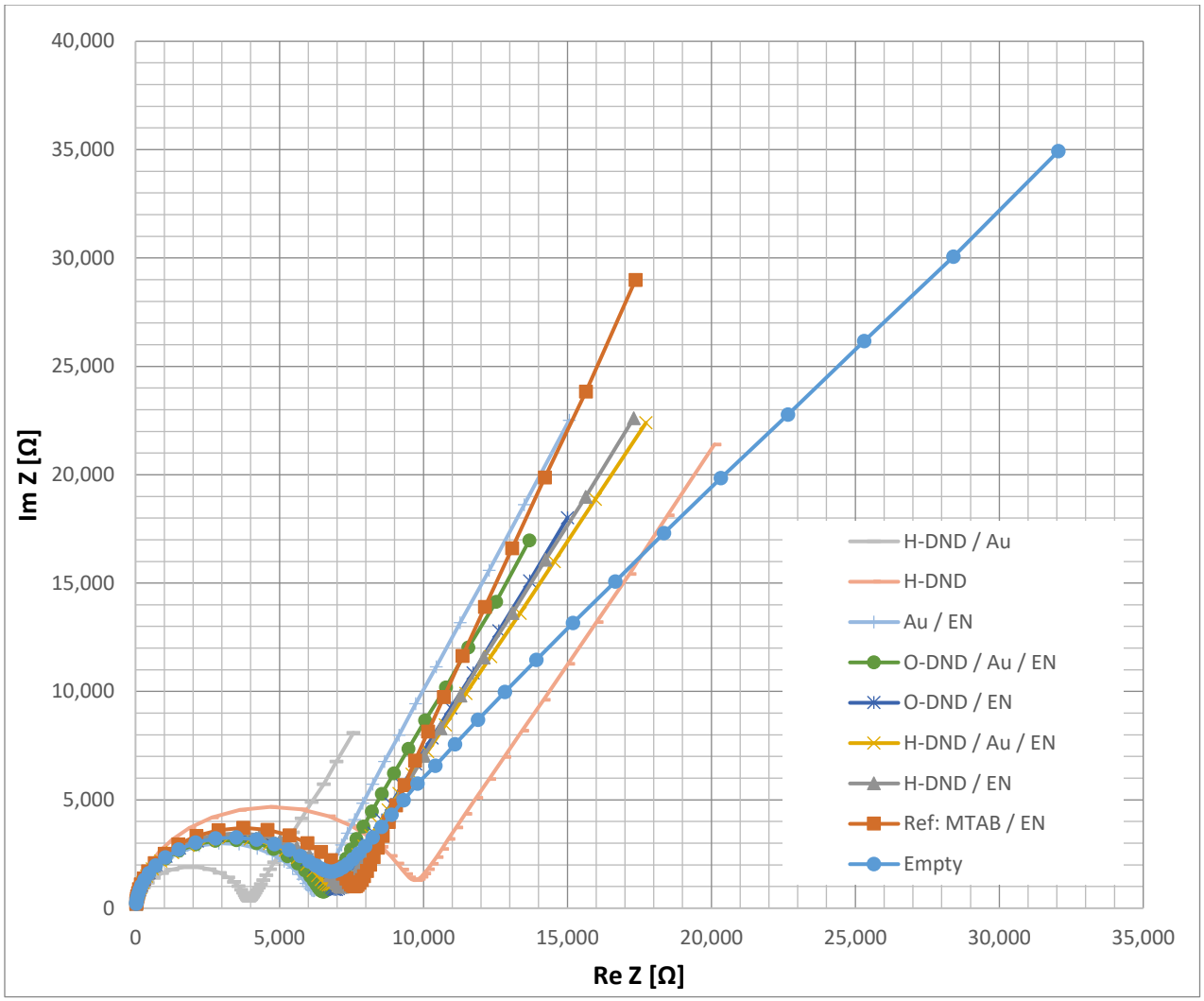

Fig 18. Nyquist Plots for IDT sensors in Test Fixture.

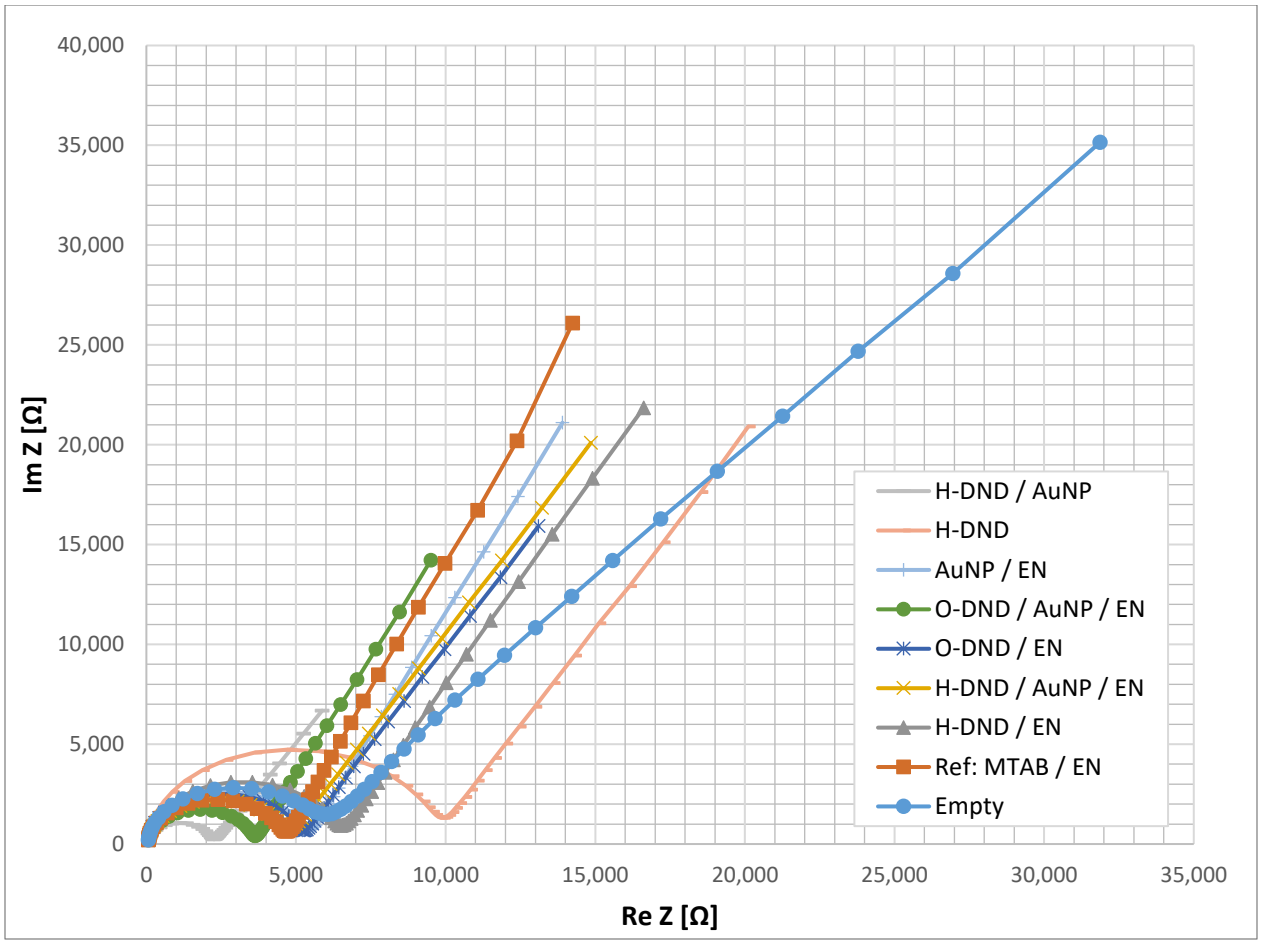

Fig 19. Nyquist Plots of IDT sensors measured in Chamber.

From Fig. 20 we can see that H-DND has more sensitivity to the modification of the layer compared to O-DND analogues in Fig. 21. The difference between the H-DND and H-DND / AuNP is about 7 times larger than the difference between O-DND and O-DND / AuNP. The AuNP has the effect of improving the electrical connectivity, which is evidenced by lowered impedance. Adding additional layer, shows to impede the analysis, such as the EN agent, which is what we would like to observe. Moreover, from Fig. 8 we can observe the improvement of impedance O-DND / AuNP / EN, by functionalizing the AuNP with MTAB. This improvement may be as a consequence of increased conjugation of EN agent molecules with AuNP.

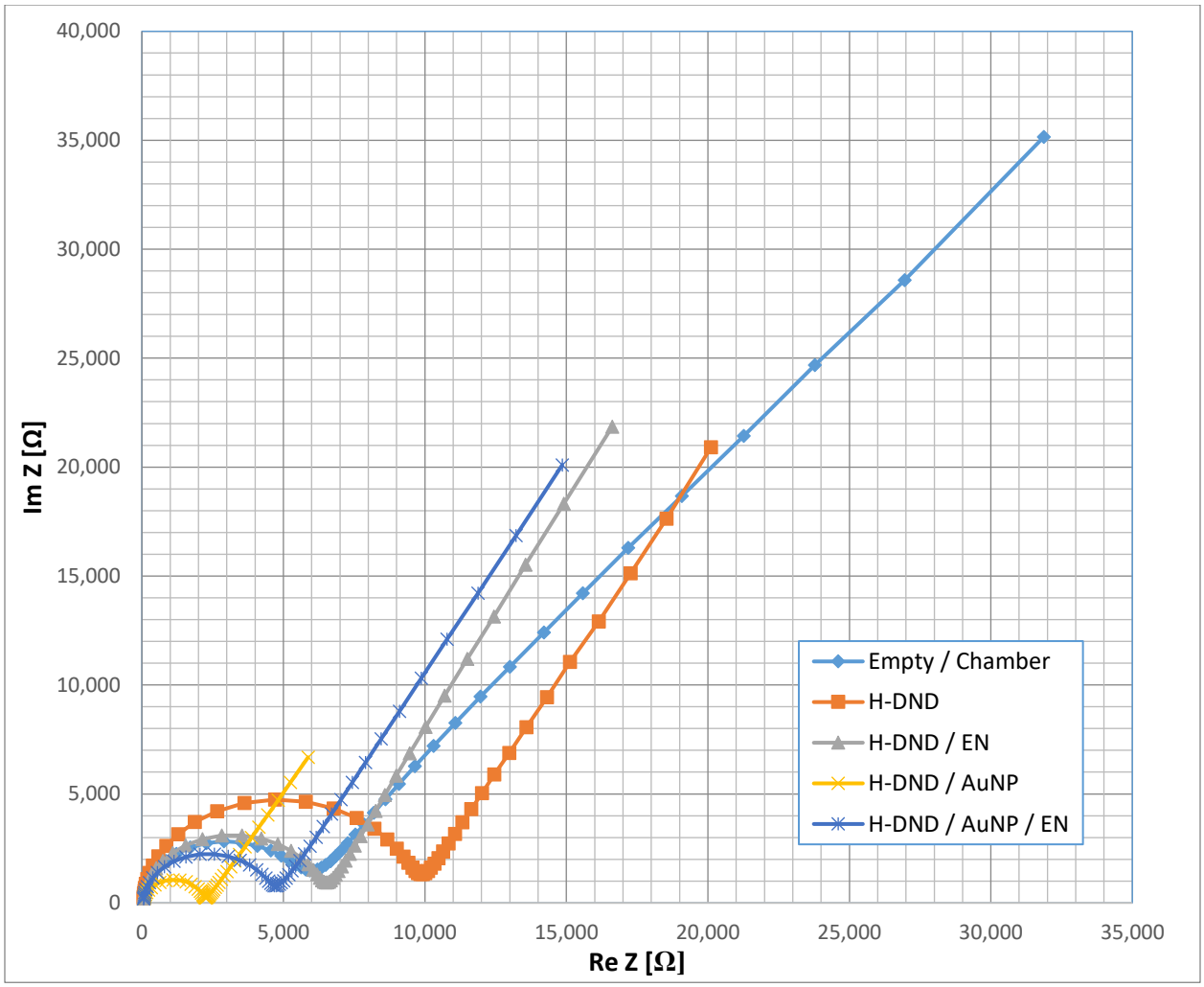

Fig 20. Comparison between different combinations of H-DND based layers.

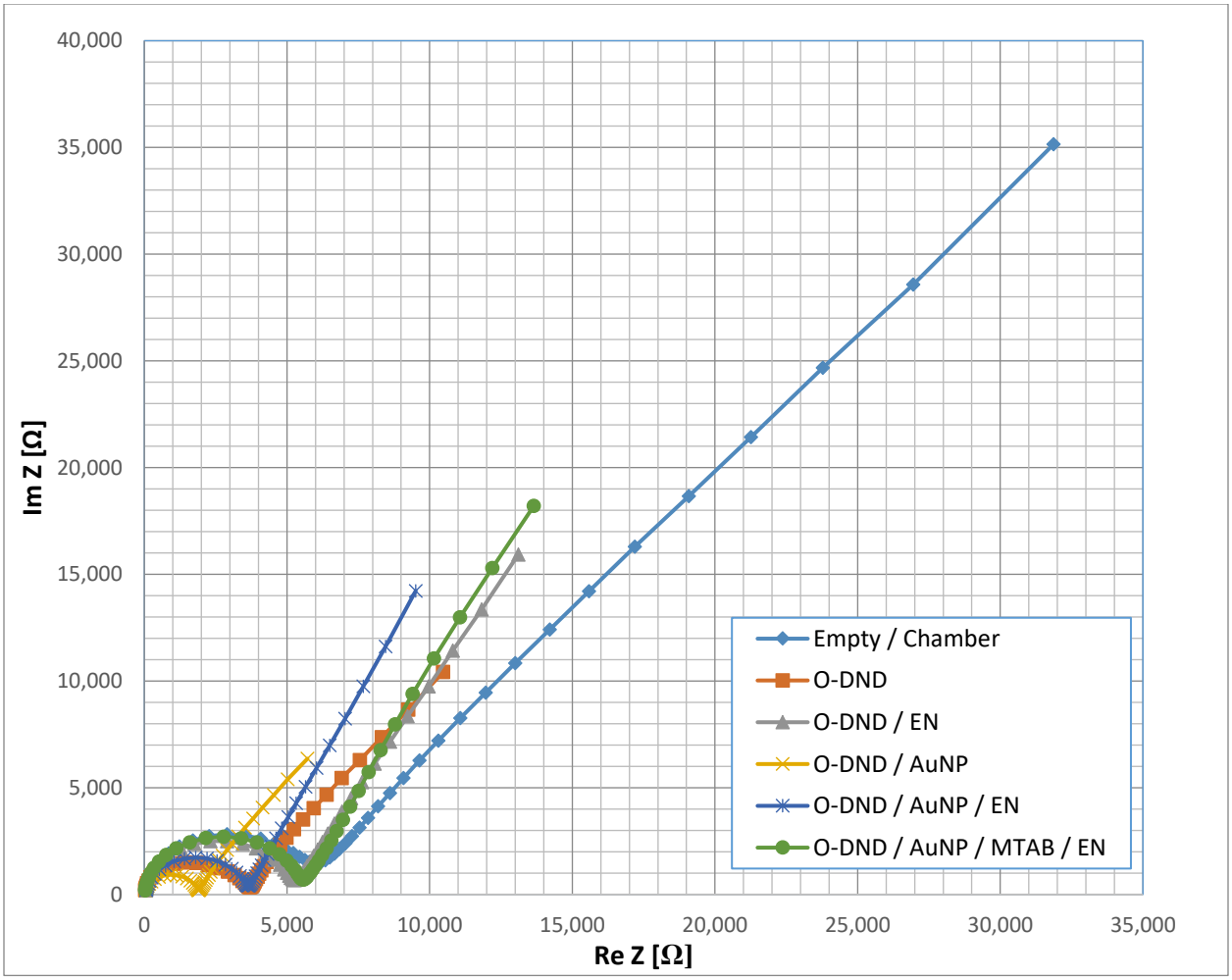

Fig 21. Comparison between different combinations of O-DND based layers.

9. Model for the measurements

In many areas of science, the measured data produced by different measurement techniques, including EIS, are interpreted in terms of "models" [8]. In our case, the model takes the form of an equivalent circuit, that attempts to represent the pattern of data, gathered from our measurements, in terms of a mathematical expression. So, by substituting the right parameters in our mathematical expression, we are able to reproduce the individual impedance curves. The EC at Fig. 22 was obtained from a parallel research work [15].

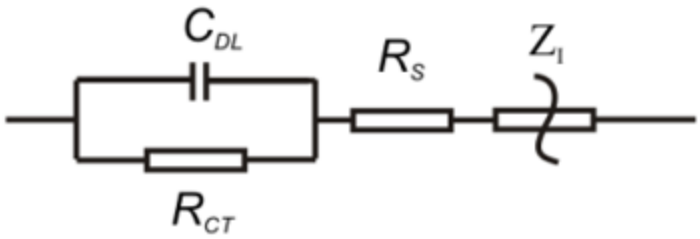

Fig 22. EC model, which describes the behavior of the sensor impedance [15].

In Fig. 22 R_S is the sum of the lead and electrolyte resistances, R_{CT} is charge transfer resistance, C_{DL} is double layer capacitance and Z_I is impedance of the double layer capacitance in the presence of surface roughness effects. Z_I has the form (13) [15], where f is the frequency of the signal:

$$Z(f) = R_s + \frac{1}{\frac{1}{R_{CT}} + \mathrm{j}\,\omega\, C_{DL}} + Z_I \tag{12}$$

$$Z_I = \frac{a}{f^{\alpha}} + j\frac{b}{f^{\beta}} \tag{13}$$

The parameters a,b,α and β, were obtained using curve fitting technique. The curve fitting was done in a computer software Wolfram Mathematica. The uncertainty produced from curve fitting was calculated to be less than 1 %. It was calculated as square root of sum of squares of deviations divided by sum of squares of impedances [15].

10. Conclusion

The objectives that were carried out throughout the thesis work are the following:

1. Gathering information and analysis on the topics of interdigitated sensors, NP, impedance measurement and EIS.
2. Familiarization with the laboratory equipment, such as the LCR meter, its setup and procedures for impedance measurement.
3. Measuring the impedance of numerous sensors with different kind of sensing layers, analysis and comparison of the results, and description of a model.

The study and research of label-free systems and sensors plays an essential role in the development fast and efficient drug analysis in the medical industry. Not only method of such analysis was explored in this thesis, but the enhancement and improvement of the analysis by utilizing NPs of different nature were covered. Specifically, impedance method was used to evaluate the electrochemical states of the sensor with different

combinations of species. The DND particles were used in order to increase the surface area for the analyte sedimentation. Also, H-terminated DNDs, provided with higher sensitivity to different layers. However, due to the difference between the results from O-DND and H-DND, more is needed to be understood about the chemical properties and their manifestaion in the physical properties for these different surface terminations. The AuNP had the effect of decreasing the impedance, while functionalization of with MTAB seems to indicate better binding of the analyte EN, when comparing the layers of EN on top of functionalized AuNP, as opposed to, regular AuNP. The two separate measurement in different setups, such as the chamber and test fixture requires more investigation, to find an ideal measurement bench. The measurements in chamber were consistent and provided clearer separation of impedances and therefore were included for comparison. Although a model was investigated [15], which replicates the phenomenon of the impedance at the sensor surface, there is still much to be understood about the mechanism itself for indepth analysis of the data. This thesis presented an entrance level work into this research, but more improvements and exploration is planned ahead and ,hopefully, will come into fruition.

11. References

[1] http://www.tesla-blatna.cz/soubory/datasheet_bi2.pdf

[2] Arnault J. Ch., Nanodiamonds, Elsevier, Eastbourne, UK, 2017, ISBN 978-0-323

[3] Vadym N. Mochalin ,Olga Shenderova ,Dean Ho,Yury Gogotsi, The properties and applications of nanodiamonds, Nature Nanotechnology, Jan 2012, Vol. 7 Issue 1, p11-23. 13p, ISSN: 1748-3387

[4] Heather K. Hunt and Andrea M. Armani, Label-free biological and chemical sensors, Nanoscale, 2010,2, 15441559

[5] Ian I. Suni, Impedance methods for electrochemical sensors using nanomaterials, TrAC Trends in Analytical Chemistry, Volume 27, Issue 7, 2008, Pages 604-611, ISSN 0165-9936

[6] Ha-Wook Jung, Young Wook Chang, Ga-yeon Lee, Sungbo Cho, Min-Jung Kang, Jae-Chul Pyun, A capacitive biosensor based on an interdigitated electrode with nanoislands, Analytica Chimica Acta, Volume 844, 2014, Pages 27-34, ISSN 0003-2670

[7] https://www.bbisolutions.com/en/amfile/file/download/file_id/151/product_id/259/

[8] Digby D. Macdonald, Reflections on the history of electrochemical impedance spectroscopy, Electrochimica Acta, Volume 51, Issues 8–9,2006, Pages 1376-1388, ISSN 0013-4686

[9] Yeh Y-C, Creran B, Rotello VM. Gold Nanoparticles: Preparation, Properties, and Applications in Bionanotechnology. *Nanoscale*. 2012;4(6):1871-1880

[10] https://www.hioki.com/file/cmw/hdCatalog/4797/pdf/?action=browser&log=1&lang=en

[11] https://www.hioki.com/file/cmw/hdCatalog/4654/pdf/?action=browser&log=1&lang=en

[12] https://www.hioki.com/file/cmw/hdTechnicalDataEn/46/attached_file/?action=browser&log=1&lang=en

[13] https://www.bbisolutions.com/en/amfile/file/download/file_id/151/product_id/259/

[14] Eugenie Nepovimova, Elisa Uliassi, Jan Korabecny, Luis Emiliano Peña-Altamira, Sarah Samez, Alessandro Pesaresi, Gregory E. Garcia, Manuela Bartolini, Vincenza Andrisano, Christian Bergamini, Romana Fato, Doriano Lamba, Marinella Roberti, Kamil Kuca, Barbara Monti, and Maria Laura Bolognesi, Multitarget Drug Design Strategy: Quinone–Tacrine Hybrids Designed To Block Amyloid-β Aggregation

and To Exert Anticholinesterase and Antioxidant Effects, *Journal of Medicinal Chemistry* **2014** *57* (20), 8576-8589

[15] Bohuslav Rezek, Ilona Ali Bláhová, Ivana Pilarčíková, Tomáš Finsterle, Jan Kyncl, Štěpán Potocký, Egor Ukraintsev, Štěpán Stehlík, Alexander Kromka, Eugenie Nepovimová , Jan Korábečný , Kamil Kuča, Electronic detection of drug molecules enhanced by nanodiamond-based impedance sensors, Submitted 2018